Journal of Computational Physics 231 (2012) 676–692

Contents lists available at SciVerse ScienceDirect

Journal of Computational Physics

journal homepage: www.elsevier.com/locate/jcp

Droplet size and velocity distributions for spray modelling

D.P. Jones [a,*], A.P. Watkins [b,1]

[a] School of Engineering and Materials Science, Queen Mary, University of London, London E1 4QD, United Kingdom
[b] School of Mechanical, Aerospace and Civil Engineering, University of Manchester, Manchester M60 1QD, United Kingdom

ARTICLE INFO

Article history:
Received 29 November 2010
Received in revised form 29 September 2011
Accepted 30 September 2011
Available online 12 October 2011

Keywords:
Spray
Moments
Modelling
Droplet size distribution
Droplet velocity profile

ABSTRACT

Methods for constructing droplet size distributions and droplet velocity profiles are examined as a basis for the Eulerian spray model proposed in Beck and Watkins (2002,2003) [5,6]. Within the spray model, both distributions must be calculated at every control volume at every time-step where the spray is present and valid distributions must be guaranteed. Results show that the Maximum Entropy formalism combined with the Gamma distribution satisfy these conditions for the droplet size distributions. Approximating the droplet velocity profile is shown to be considerably more difficult due to the fact that it does not have compact support. An exponential model with a constrained exponent offers plausible profiles.

1. Introduction

A computational spray model was presented in [6] which avoided the need to segregate the local droplet number distribution into parcels of identical droplets. Characteristics of the spray were instead obtained via the transportation of the third and fourth moments (μ_2 and μ_3) of the local droplet distribution and their moment-averaged momentums. From these moments, a special form of the Gamma distribution with one fixed parameter was used to recover the underlying local droplet size distribution in order for the computation of hydrodynamic forces acting on the droplets, such as inter-phase drag, droplet break-up and inter-droplet collisions. Evaluation of these forces requires moments integrated over parts of the droplet size range, hence the transported moments alone without a distribution model do not suffice to close the spray model.

Whilst this novel spray model was shown to perform reasonably well, there were a number of outstanding issues still to be addressed. Among them were two which this paper examines. They are the limited capacity to represent a local underlying droplet size distribution based on one free parameter and the assumption that local droplets travel at the same speed. Initial work on the first issue was taken up in [16], where the form of the distribution was revised by implementing the standard Gamma distribution whose two free parameters were obtained from the second, third and fourth moments. Unfortunately, the gain in representing a slightly broader range of distributions leads to a significant reduction in the stability of the spray model algorithm. Instability was partly attributed to the assumption of the second issue, that of uniformity of local droplet speed. This assumption had the effect of causing hydrodynamic terms in the transport equations to be over-estimated in the small droplet size range because the velocity difference between the spray and the surrounding gas was too great. As a result of this over-estimation, lower order moment transportation tended to significantly lag behind the high order moments after a relatively long period, producing excessively large mean droplet sizes at the leading edge of the spray. A non-linear droplet velocity profile was proposed in [10] and this allied with the standard Gamma distribution approach

* Corresponding author. Tel.: +44 (0) 20 7882 5512.
E-mail addresses: dominic.jones@qmul.ac.uk (D.P. Jones), paul.watkins@manchester.ac.uk (A.P. Watkins).
[1] Tel.: +44 (0) 161 306 3706.

0021-9991/$ - see front matter © 2011 Elsevier Inc. All rights reserved.
doi:10.1016/j.jcp.2011.09.030

was implemented and preliminary simulations of spray model were presented. Very little analysis was performed on the proposed profile in that work and stability was only marginally improved.

This paper primarily presents an analysis and comparison of the more sophisticated distribution recovery methodologies in the literature and some advances in implementing them. From the analysis a suitable method is sought which can rapidly and accurately represent the local droplet distribution for the moments-based spray model. The applicability of this work also extends to other moments-based modelling such as aerosol modelling [14]. Secondly, a similar analysis is performed on a range of droplet velocity profiles in order to assess their capacity to represent sensible profiles reliably. This work is particular to spray models. Sections 2–4 present a review of moments and the literature on the models being implemented and assessed.

2. Moments of a continuous distribution

2.1. Moments about the origin

The simplest definition of moments of a continuous distribution, $\phi(r)$, is the moments about its origin, defined as

$$\mu_i = \mu_0 \int_r \phi(r) r^i \, \mathrm{d}r \tag{1}$$

whereby the first moment (when $i = 0$) simply returns the integral of the distribution. If the distribution is a probability density function, $\mu_0 = 1$; for a number density, the total number per unit volume; and for the volume density, the sum of the individual volumes per unit volume, etc.

Assuming the distribution to represent the range of (spherical) droplet sizes within a given volume, the first four moments of the distribution have physical interpretations. In the case where the distribution is not a probability density, moments are often normalized by the constant, μ_0, giving the normalized moments about the origin (Table 1).

$$\hat{\mu}_i = \frac{\mu_i}{\mu_0} \tag{2}$$

Moment ratios are of interest, providing definitions of different kinds of mean values based on the moments. This is defined as

$$r_{ji} = \left(\frac{\mu_j}{\mu_i}\right)^{\frac{1}{j-i}} \tag{3}$$

A moment ratio frequently cited in literature for characterizing spray droplet size is the Sauter mean radius (SMR), r_{32}.

2.2. Moments about the mean

From the moments about the origin, moments about the mean (or centralized moments) are defined as

$$\mu'_i = \int_r (r - r_{10})^i \phi(r) \mathrm{d}r \tag{4}$$

whereby the first central moment (when $i = 1$) is zero. The second moment (Eq. (6)) defines the variance of the distribution and the third and fourth moments (Eqs. (7) and (8)) are used to define the standardized moments.

$$\mu'_1 = 0 \tag{5}$$

$$\mu'_2 = \hat{\mu}_2 - r_{10}^2 \tag{6}$$

$$\mu'_3 = \hat{\mu}_3 - 3r_{10}\hat{\mu}_2 + 2r_{10}^3 \tag{7}$$

$$\mu'_4 = \hat{\mu}_4 - 4r_{10}\hat{\mu}_3 + 6r_{10}^2\hat{\mu}_2 - 3r_{10}^4 \tag{8}$$

Table 1
Interpretation of moments.

Quantity (per unit volume)	Moment relation
Total number of droplets	μ_0
Sum of the radii	μ_1
Sum of the surface areas	$4\pi\mu_2$
Sum of the volumes	$\frac{4}{3}\pi\mu_3$

2.3. Standardized moments

To calculate skewness and kurtosis of the distribution, the standardized moments are required. These moments are defined as

$$\mu_i'' = \frac{\mu_i'}{\sigma^i} \tag{9}$$

where the standard deviation, $\sigma = \sqrt{\mu_2'}$. From the definition of standard deviation, the condition

$$\mu_2' > 0 \tag{10}$$

is imposed. As this (the variance) tends to zero, the shape of the distribution will become more peaked. Skewness and kurtosis are defined as

$$\gamma_1 = \mu_3'' \tag{11}$$
$$\gamma_2 = \mu_4'' - 3 \tag{12}$$

The above explanation shows how the common parameters for characterizing a distribution relate to the primary definition in Eq. (1) of the distribution's moments. It also provides an indication of how many moments (about the origin) are typically required to adequately describe a distribution in terms of these common parameters; the first five moments, μ_0–μ_4, are required to calculate the mean, variance, skewness and kurtosis of a distribution.

No limits for the moments about the mean are imposed, except for Eq. (10). However, additional limits are required on the moments to ensure the representation of sensible distributions.

3. Distribution construction methods

Moments of a continuous distribution have been discussed without mentioning the form of the distribution itself, assuming it is already somehow known. In the spray model of [6], the distribution is not initially known and a means of determining the underlying probability density function is required given a finite set of its moments. If this given set of moments does not include the first moment, μ_0, this has to be determined first.

This kind of problem is classified as an inverse problem and is generally ill-posed; usually being deficient on one or more of the conditions of a well-posed problem (that of existence, uniqueness and stability) and as a result the computation of the solution is ill-conditioned [8].

A number of methods are available for prescribing the general form of a probability density function (PDF), such as assuming an a priori form [16,8], using polynomial fitting [8,13] or the Maximum Entropy formalism [2,15]. Each method has different characteristics but none of them possesses all the qualities of a well-posed solution. Whichever method is used, the specific form is determined through knowledge of the moments.

The following presents five methods of solving this inverse problem, though none of them suitably combines the requirements of being computationally inexpensive and robust, accurate and with minimum constraints on the shape of the distribution. In addition, only one method provides a means for calculating μ_0 from the available moments before the distribution is solved.

3.1. Normalization and limits

For some closure methods, the moments require normalizing. This is done either to ensure the distribution is between certain limits such as the interval of 0 to 1, or more generally, to reduce the numerical difference between moments. In either case, a normalizing length scale is required. Using the ratio of any pair of successive moments a normalization radius r_n can be defined,

$$r_n = \frac{\mu_{i+1}}{\mu_i} \tag{13}$$

This radius can then be used to provide a sensible range in which the upper limit lies. From numerical tests, the upper limit can be assumed to lie in the range $r_n < r_u < 3.5\, r_n$ (for $i = 2$) and the lower limit, r_l, set to zero. In two of the methods presented where the limits are required [8,13], accuracy of the estimated interval significantly effects the accuracy of the resulting distribution. To obtain accurate limits (only the upper limit is corrected), an iterative procedure is required.

Upon establishing a normalizing length scale, r_n, and before the closure method is called, linear normalization of the moments is performed by substitution of $x = \frac{r}{r_n}$ into Eq. (1), giving

$$\frac{\mu_i}{\mu_0 r_n^{1+i}} = \int_{r_n x} \phi(r_n x) x^i \, \mathrm{d}x \tag{14}$$

3.2. Maximum Entropy distribution

The probability density function is approximated as [15]

$$\phi(r) \approx p(r) \exp\left[-\sum_{i=0}^{N-1} \lambda_i r^i\right] \tag{15}$$

where N is the number of moments available and $\lambda_0,\ldots,\lambda_{N-1}$ are the Lagrangian multipliers and $p(r)$ is the 'preconditioning' approximate distribution. Different possible forms of $p(r)$ are listed in Table 2.

Substituting Eq. (15) into Eq. (1) provides N equations with N unknown multipliers (Eq. (16))

$$f_j(\underline{\lambda}) = \int_r r^j p(r) \exp\left[-\sum_{i=0}^{N-1} \lambda_i r^i\right] \mathrm{d}r = \frac{\mu_j}{\mu_0} \tag{16}$$

In order to solve the set of equations, $f_j(\underline{\lambda})$ is approximated as a first-order Taylor series, using the general form for functions with several arguments;

$$f_j(\underline{\lambda}) = \sum_{k=0} \frac{1}{k!} \frac{\mathrm{d}^k}{\mathrm{d}\underline{\lambda}^k} [f_j(\underline{\lambda}^0)] \cdot (\underline{\lambda} - \underline{\lambda}^0)^k \tag{17}$$

$$\approx f_j(\underline{\lambda}^0) + \frac{\mathrm{d}}{\mathrm{d}\underline{\lambda}} [f_j(\underline{\lambda}^0)] \cdot (\underline{\lambda} - \underline{\lambda}^0) \tag{18}$$

where the gradient of $f_j(\underline{\lambda})$ is

$$\frac{\mathrm{d}}{\mathrm{d}\lambda_k} [f_j(\lambda_k)] = -\int_r r^k r^j p(r) \exp\left[-\sum_{i=0}^{N-1} \lambda_i r^i\right] \mathrm{d}r \tag{19}$$

Rearranging Eq. (18) leads to a system of linear equations. Before the solution to these equations can be formed, the gradients must be calculated by performing numerical integration. Both tasks can be accomplished using standard mathematical library packages. Initial multipliers, $\underline{\lambda}^0$, are typically set to zero.

3.3. Splines distribution

This method considers the distribution as a summation of N_{spl} splines of degree N_{deg}, where each spline is defined in the interval $[r_i, r_{i+1}]$, as [8]

$$\phi(r) \approx \sum_{i=1}^{N_{spl}} \sum_{j=0}^{N_{deg}} \lambda_{i,j} (r - r_i)^j \tag{20}$$

whereby the number of splines is dependent on the number of available moments, N_μ, as

$$N_{spl} = N_{deg} + N_\mu \tag{21}$$

The degree of the splines is optional, but cubic splines are usually employed. Boundary conditions at r_1 and $r_{N_{spl}+1}$ and differentiability conditions at internal nodes ($r_i,\ i = 2,\ldots,N_{spl}$) provide $(N_{deg}+1)N_{spl} - N_\mu$ equations with $(N_{deg}+1)N_{spl}$ unknowns, $\lambda_{i,j}$. The additional equations are derived from substitution of Eq. (20) into Eq. (1), which can be integrated analytically. Here, the integrand is expanded using the binomial theorem, resulting in

$$\int_{r_i}^{r_{i+1}} (r - r_i)^j \mathrm{d}r = \sum_{k=0}^{j} \binom{j}{k} (r_{i+1}^{j+k+1} - r_i^{j+k+1})(-r_i)^{\frac{j-k}{j+k+1}} \tag{22}$$

From the equations a system of linear equations can be written. With increasing the number of moments used, the condition number of the matrix formed rapidly tends towards infinity. In order to obtain a sensible solution to the system of equations,

Table 2
Approximate distribution functions.

Type	$p(r)$
Uniform	1
Mean value	r_{10}
Exponential	$\frac{1}{r_{10}} \exp\left(-\frac{r}{r_{10}}\right)$
Rayleigh	$\frac{r}{s^2} \exp\left(-0.5\frac{r^2}{s^2}\right)$, where $s = r_{10}\sqrt{0.5\pi}$
Beck [4]	$16\frac{r}{r_{32}^2} \exp\left(-4\frac{r}{r_{32}}\right)$

singular value decomposition is required. This approach provides a means of ignoring the small singular values, which may be regarded as numerical noise. In order to ensure that the singular values which are disregarded do not result in discontinuities in the resulting distribution, all the equations relating to the nodal conditions are numerically weakened by the constant ω^l, where l is the order of the differentiability condition.

To produce a physically sensible and accurate distribution, both the limits of the distribution and the singular value cut-off need to be determined. The former is done iteratively by examining the tails of the distribution. The latter can either be iteratively increased until the distribution is physically sensible or the cut-off can be found non-iteratively by inspection of the singular values. If the first choice is adopted then the solution scheme becomes a nested iterative scheme, whilst the latter method avoids the nested iteration, but may not produce an equally accurate result. Here, the non-iterative approach is taken.

3.4. Laguerre distribution

The generalized Laguerre polynomial of degree i and order k is given by

$$L_i^k(r) = \frac{r^k e^r}{i!}\frac{\mathrm{d}^i}{\mathrm{d}r^i}(r^{i+k}e^{-r}) = \sum_{j=0}^{i}\frac{(-1)^j}{j!}\binom{i+k}{i-j}r^j \tag{23}$$

and is orthogonal over the interval $[0,\infty]$ with respect to the weighting function $w_k(r) = r^k e^{-r}$,

$$\int_0^\infty w_k(r)L_i^k(r)L_j^k(r)\mathrm{d}r = \frac{(j+k)!}{j!}\delta_{ij} \tag{24}$$

Since the polynomials are orthogonal over this interval, the normalization of the moments needs to be such that the normalized radius scales well with the Laguerre polynomial coefficients. From considering the function $x\exp(-x)$, the upper limit can be approximated as lying between 15 and 20.

By exploiting the orthogonality property in Eq. (24), the probability density function can be defined as

$$\phi(r) \approx w_k(r)\sum_{i=0}^{N_\mu-1}\lambda_i^k L_i^k(r) \tag{25}$$

Substituting Eq. (25) into Eq. (24) provides the equation for calculating the coefficients λ_i^k as a function of the available moments,

$$\lambda_i^k = \sum_{j=0}^{i}\frac{(-1)^j}{j!}\binom{i+k}{i-j}\mu_j \tag{26}$$

It is worth noting that Eqs. (23) and (26) have exactly the same form, making the implementation of the method very simple.

3.5. Legendre distribution

This method is based on shifted Legendre polynomials for the interval $[0,1]$, and is given in [13]

$$L_i(r) = \frac{1}{i!}\frac{\mathrm{d}^i}{\mathrm{d}r^i}((r^2-r)^i) = \sum_{j=0}^{i}(-1)^j\binom{i}{j}\binom{i+j}{j}r^j \tag{27}$$

and is orthogonal, giving the condition

$$\int_0^1 L_i(r)L_j(r)\mathrm{d}r = \frac{1}{2j-1}\delta_{ij} \tag{28}$$

The probability density function is then defined as

$$\phi(r) \approx \sum_{i=0}^{N_\mu-1}(2i+1)\lambda_i L_i(r) \tag{29}$$

where

$$\lambda_i = \sum_{j=0}^{i}(-1)^j\binom{i}{j}\binom{i+j}{j}\mu_j \tag{30}$$

3.6. A priori distributions

There are a number of possible distributions which could be assumed to represent the underlying probability density function, such as the Log-Normal, Gamma, Beta and the Rayleigh distributions. Here, only the Gamma distribution will be developed.

The Gamma distribution is defined as

$$\phi(r) = \frac{r^{k-1}}{\Gamma(k)\theta^k} \exp\left(-\frac{r}{\theta}\right) \tag{31}$$

where

$$\Gamma(k)\theta^k = 1 \tag{32}$$

by definition. Combining Eqs. (31) and (1) gives

$$\begin{aligned}\frac{\Gamma(k)\theta^k \mu_j}{\mu_0} &= \int_0^\infty r^{k-1+j} \exp\left(-\frac{r}{\theta}\right) \mathrm{d}r = \left[-\theta r^{k-1+j} \exp\left(-\frac{r}{\theta}\right)\right]_0^\infty + \theta(k-1+j)\int_0^\infty r^{k-2+j} \exp\left(-\frac{r}{\theta}\right)\mathrm{d}r \\ &= \frac{\theta(k-1+j)\mu_{j-1}}{\mu_0}\end{aligned} \tag{33}$$

which simplifies to

$$\frac{\mu_{j+1}}{\mu_j} = \theta(k+j) \tag{34}$$

From Eq. (34), the parameters can be related to three consecutive moments by

$$k = \frac{j\left(1 - \frac{\mu_{j+2}\mu_j}{\mu_{j+1}^2}\right) + 1}{\frac{\mu_{j+2}\mu_j}{\mu_{j+1}^2} - 1} \tag{35}$$

$$\theta = \frac{\mu_{j+1}}{\mu_j(k+j)} \tag{36}$$

To ensure the denominator of the above equation remains unconditionally positive, limits are set on parameter k such that $1.5 < k < 20$. Moments of the Gamma distribution can be calculated by

$$\mu_\alpha|_{r_l}^{r_u} = \mu_0 \theta^\alpha \frac{\Gamma(k+\alpha)}{\Gamma(k)} \left[\gamma\left(k+\alpha, \frac{r_u}{\theta}\right) - \gamma\left(k+\alpha, \frac{r_l}{\theta}\right)\right] \tag{37}$$

where $\gamma(k,x)$ is the lower incomplete Gamma function.

4. Droplet velocity profile construction methods

The manner in which intensive properties of the droplets, such as temperature and velocity, vary with droplet size may be captured in a similar way to the moments capturing the variation of the underlying distribution. By averaging such a property, $\psi(r)$, over the probability density function, moment averaged quantities, Ψ_i, are obtained by

$$\Psi_i = \frac{\int_r \phi(r) r^i \psi(r) \mathrm{d}r}{\int_r \phi(r) r^i \mathrm{d}r} \tag{38}$$

$$= \frac{\mu_0}{\mu_i} \int_r \phi(r) r^i \psi(r) \mathrm{d}r \tag{39}$$

In [12] it was shown that whilst the determination of the probability density function in Eq. (1) is ill-conditioned, determination of functionals like $\psi(r)$ in Eq. (39) is well conditioned and can be reliably determined, assuming that Ψ_i and $\phi(r)$ are known.

4.1. Stabilized closure

To aid the solution of the underlying distribution from the knowledge of the moments by defining the distribution, $\phi(r)$ to be the product of a known approximation to $\phi(r)$ and a second distribution, to be determined, i.e.

$$\phi(r) \simeq p(r)\phi(r)^* \tag{40}$$

where $p(r)$ is the known approximation. The role of $p(r)$ is very much analogous to the role of a preconditioning matrix in solving a system of linear equations: if $p(r) = 1$, the initial problem is recovered and so is of no benefit, but if $p(r)$ takes on a useful form, for example, a Gaussian distribution, the convergence of $\phi(r)^*$ is stabilized and accelerated.

4.2. Exponential profile

The first method for approximating the droplet velocity profile (Eq. (41)) assumes that for small droplets, their velocity, $\vec{v}_d$, increases rapidly from the surrounding gas velocity, $\vec{v}$, with increasing droplet radius and for large droplets, velocity increases slowly (for $0 < b < 1$)

$$\vec{v}_d(r) = \vec{v} + \vec{a}_i r^b \tag{41}$$

The coefficient, $\vec{a}_i$, is determined by substituting Eq. (41) into Eq. (39), giving

$$\vec{a}_i = (\vec{V}_{d,i} - \vec{v})\frac{\mu_i}{\mu_{i+b}} \tag{42}$$

where $\vec{V}_{d,i}$ is the ith moment averaged velocity. Eq. (41) implies that an individual drop velocity is a function of moments, which is not true. To compensate for this inconsistency, the index i is taken to be 3, weighting the distribution on the behaviour of the volumetric moment transportation.

4.3. Polynomial profile

The second method is to not take into account the surrounding gas velocity, but make use of all the available moment averaged velocities to obtain a functional form for the droplet velocity variation. The simplest form is to consider an Nth degree polynomial, where there are $N + 1$ moment averaged velocities available. This is certainly not the best form (potentially forming an ill-conditioned problem for high order polynomials), but serves as a starting point for forming non-linear functions from a complete set of moment-averaged data

$$\vec{v}_d(r) = \sum_{j=0}^{N} \vec{a}_j r^j \tag{43}$$

Substituting Eq. (43) into Eq. (39) results in a system of linear equations for solving the unknown coefficients, $\vec{a}_j$.

A variation on this method is to define the constant, a_0, as a function of the continuum phase velocity and the lowest available moment averaged velocity, such as

$$\vec{a}_0 = \lambda\vec{v} + (1 - \lambda)\vec{V}_{d,0} \tag{44}$$

where $0 < \lambda < 1$ and change the summation in Eq. (43) to $j = 1, \ldots, N + 1$. Coefficients of Eq. (44) are solved in a similar manner as above.

4.4. Maximum Entropy formalism

Finally, as a third method, the Maximum Entropy formalism may be used as a means to construct the velocity profile. The Maximum Entropy formalism is represented here in its general form in order to describe the solution of both the probability density function, $\psi(r)$, and the droplet velocity profile, $v_d(r)$. The continuous function to be recovered is defined as

$$q(r) = p(r)\exp\left[-\sum_{i=0}^{N-1}\lambda_i e_i(r)\right] \tag{45}$$

where $q(r)$ is the approximated distribution. The preconditioning function, $p(r)$, and the external function, $e_i(r)$, are defined according to the type of distribution required. For constructing the PDF, $e_i(r) = r^i$, and for the velocity profile, $e_i(r) = \psi(r)r^i$. To solve the droplet velocity profile, $v_d(r)$, substituting Eq. (45) into Eq. (39) and normalizing the result gives

$$f_j(\underline{\lambda}) = \frac{1}{V_{d,0}}\int_r e_j p(r)\exp\left[-\sum_{i=0}^{N-1}\lambda_i e_i(r)\right]\mathrm{d}r = \frac{\mu_j}{\mu_0}\frac{V_{d,j}}{V_{d,0}} \tag{46}$$

which can then be solved in the same way as presented earlier.

5. Implementation and assessment of distribution methods

To determine the most suitable method for recovering the probability density function from a finite set of its moments, the methods outlined in Section 2.2 (except the Gamma distribution) are tested by comparing a range of recovered PDFs to the actual PDFs from which the initial set of moments are obtained. The most appropriate reconstruction method will be decided by how many of the sample PDFs are recovered accurately. For the reconstruction cases presented below, unimodal distributions are recovered based on its first four moments and for bimodal its first eight moments. It has been found here that to resolve a distribution mode sufficiently well, at least four moments are required.

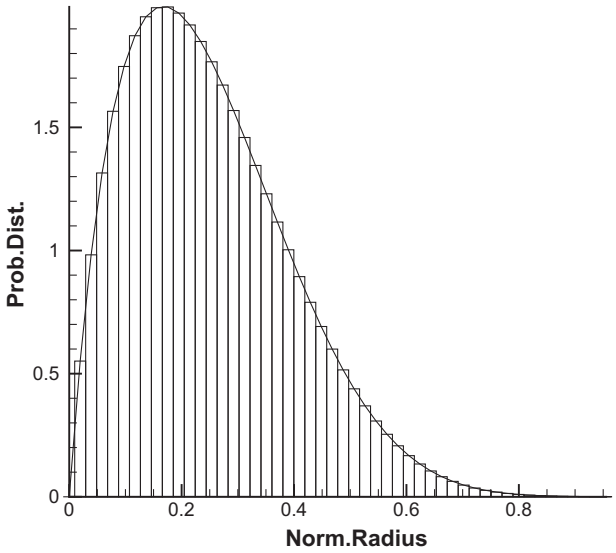

Fig. 1. Discretization of the distribution.

The procedure begins by first normalizing the radius such that the largest droplet has a normalized radius of one. The moments are also normalized by the same constant. The range $0 < r < 1$ is then segmented into a number of equal intervals (for the following cases, 50 intervals are used) as shown in Fig. 1. Once these preliminary steps are performed, the selected reconstruction method is called. Improvement in approximation can be obtained by employing a non-uniformly discretized radial range. Whilst this was considered in this work, it was not implemented due to the additional significant computational overhead required to estimate the new intervals.

5.1. Upper bound search

The construction of the splines and Legendre distributions exhibits similar behaviour as the upper limit is reduced from some initial estimate, which is currently taken as

$$r_{max} = 3.5 r_{32} \tag{47}$$

As the upper limit is reduced, the oscillations in the shape of the constructed distribution reduce and minima tend towards the positive range (Fig. 2). If the limit continues to be reduced, the distribution converges then rapidly diverges after further reduction.

From this knowledge, an algorithm is written that detects when the distribution becomes positive at all discrete radius ordinates, or to find the most accurate distribution allowing for negative values, when an unconditionally positive distribution is not found.

The Maximum Entropy method will construct the same distribution regardless of the limits, so long as the limits are not within the range of the distribution, thus requiring no iterations to optimize the upper bound estimate.

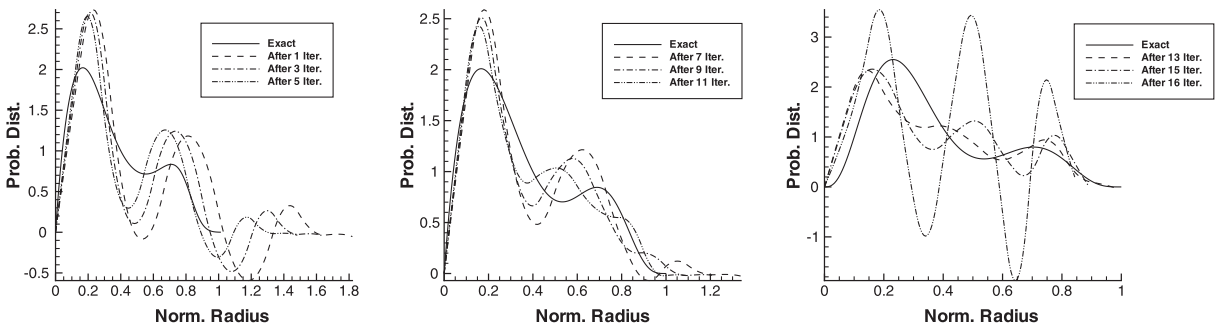

(a) Converging (b) Solution at 12 iterations (c) Diverging

Fig. 2. Effect of reducing the upper bound.

5.2. Maximum Entropy method

The possibility of defining an assumed probability density function, $p(r)$, is exploited (Table 2). The main purpose of this is to aid the convergence of the Lagrange multipliers and to improve the shape of the tails of the reconstruction. From a number of simple tests, the Exponential, Rayeigh and Beck [4] distributions were found to significantly reduce the number of iterations required to converge the solution of the Lagrange multipliers (from approximately 25 iterations to 8) compared to setting $p(r) = 1$. Little difference was found between the recovered distributions which employed the stated a priori distributions. However, using the distribution from Beck, the lower bound tail was more accurately resolved, compared with the other assumed PDFs (Exponential and Rayleigh).

5.3. Splines method

The splines method has a number of free parameters and can be solved in a number of ways. Because of this freedom, highly accurate reconstructions can be performed using this method, at the cost of determining certain free parameters iteratively for each new solution. Within the context of CFD, computational time is critical, so free parameters ought to be estimated from the outset. This generally results in sub-optimal solutions. The degree of the splines is the primary parameter. Generally, fewer moments are required if higher order splines are used, but may promote oscillations in the shape (Fig. 3).

Since the linear system of equations produced by the Splines method are highly ill-conditioned, the solution is found by calculating the pseudo-inverse. This in turn requires the matrix to be decomposed using singular value decomposition. From the produced set of singular values, the smaller values represent noise in the solution, whereas the remaining are required for the solution. One method of filtering out the singular values causing noise in the solution is to iteratively discard values, beginning with the smallest, until all the oscillations are removed. This results in a nested iterative process. Alternatively, the singular values can be filtered based on a simple criteria. The filtering technique adopted searches the ordered singular values from the largest to the smallest. If the difference between two consecutive singular values is found to be greater than an order of magnitude, all singular values after the smaller of the two is set to zero. This procedure is illustrated in Fig. 4.

5.4. Numerical integration

Once the probability density function is constructed, moments of that distribution may be required. For a priori distributions, moments are obtained as functions of their parameters (Eq. (37)). For all other methods, the distribution must be integrated numerically.

Suppose that a group of terms are functions of a single PDF and require integrating between different limits and to different orders (such as the break-up terms in [5]). To evaluate these terms the normal procedure would be to call a numerical integration subroutine for each moment calculation.

An alternative approach presented here is to perform the numerical integration once, calculating all integer moments covering the order range and limits of the required moments in a single sweep of the underlying distribution. For the simplest spray simulation case transporting four moments, employing drag, break-up and collisions models, 28 unique moments are required.

Coordinates of the constructed PDF (Fig. 5) are stored as links on a doubly linked list (Fig. 6).

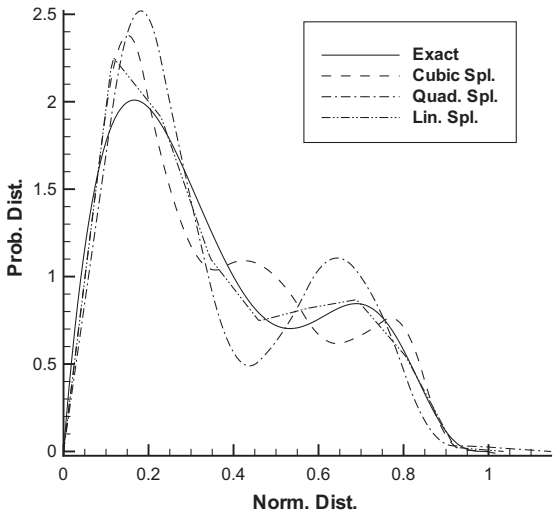

Fig. 3. Effect of splines order.

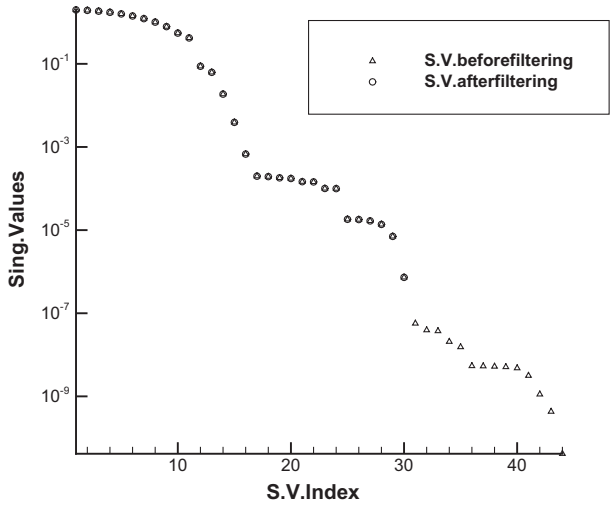

Fig. 4. Filtering singular values.

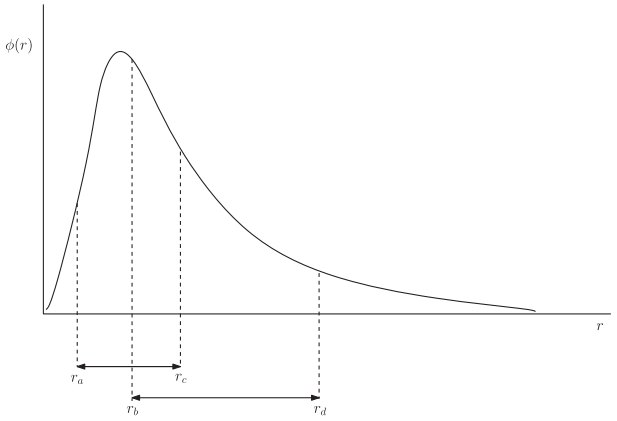

Fig. 5. Integration of a PDF between sets of limits.

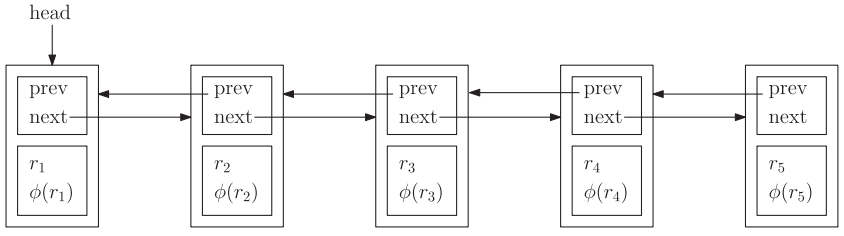

Fig. 6. Construction of integration linked list.

Pairs of integration limits are then inserted into the linked list at the appropriate position (Fig. 7) and the distribution ordinates ($\phi(r_a)$ and $\phi(r_c)$) are obtained by interpolation, forming a single chain of distribution coordinates. A pass is then made along the list, performing the elemental integration between the current link and the previous link and summating the elemental integrations between the pairs of limits.

For example, two moments are required: $\mu_{2.35}|_{r_a}^{r_c}$ and $\mu_{0.78}|_{r_b}^{r_d}$ (Fig. 5). The information then sent to the integration subroutine is *calculate moments* $\mu_0,\ldots,\mu_3$ between the limits $r_a - r_c$ *and* $r_b - r_d$, which would result in an output of eight moments grouped into two sets (μ_0 to μ_3 between r_a and r_c and μ_0 to μ_3 between r_b and r_d). The orders from 0 to 3 for the moments are requested since they span the order range of the required moments. To calculate the actual moments required, interpolation is performed between the nearest pair of integer moments using

$$\int \phi(r) r^n r^{0.m} \mathrm{d}r \approx \left(\int \phi(r) r^n \mathrm{d}r\right)^{1-0.m} \left(\int \phi(r) r^{n+1} \mathrm{d}r\right)^{0.m} \tag{48}$$

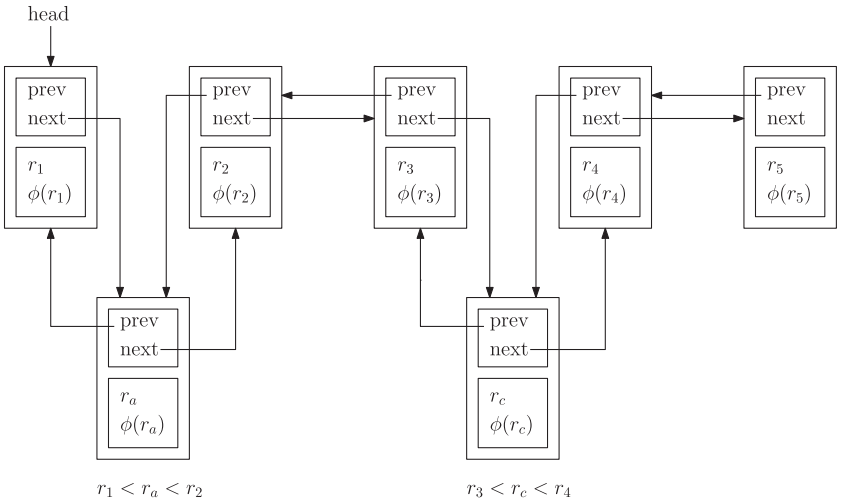

Fig. 7. Insertion of limits to the PDF list.

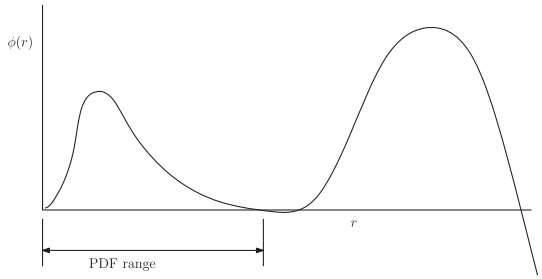

Fig. 8. Behaviour of the recovered PDF using the Laguerre method.

5.5. Sample distributions

Unimodal distributions are defined using functions

$$\phi(r) = \frac{1}{B(\alpha,\beta)} r^{\alpha-1}(1-r)^{\beta-1} \tag{49}$$

$$\phi(r) = \gamma^{\frac{1}{3}}(4r^2(1-r)^2)^{\gamma} \tag{50}$$

where Eq. (49) is used to construct positive skew distributions and Eq. (50) for negative skew distributions. These two distributions are then combined to construct bimodal distributions. The contribution by Eq. (50) is halved to produce a diminished second peak, in order to mimic realistic spray distributions.

Maximum Entropy, cubic splines and Legendre distributions are compared to the exact distribution. Different shapes of distribution are tested to show the capacity and reliability of the different methods. Results from the testing of the Laguerre distribution are not documented since the method neither recovered any of the sample distributions accurately nor conserved the input moments (Up to 20% error in the recovered moments). Its relatively poor performance is likely to be associated with the support being defined between zero and infinity, making the choice of normalization difficult, and that the resultant function (the PDF) does not diminish to zero beyond the largest droplet size but fluctuates about the axis, as in Fig. 8.

5.5.1. Unimodal

Positive skew: Fig. 9(a) shows the cubic splines method performing poorly at reconstructing the distribution with a large variance and strong negative skew. Reduction in the variance in Fig. 9(b) results in greater wiggling of the tail of the cubic splines reconstruction, whilst the other two methods perform well. Reducing the positive skew towards a bell-shaped distribution, Fig. 9(c) shows that the Legendre distribution is unable to recreate the shape, whereas the other methods do and are in good agreement. Finally, reducing the variance of Fig. 9(c) results in the distribution in Fig. 9(d). In this case the

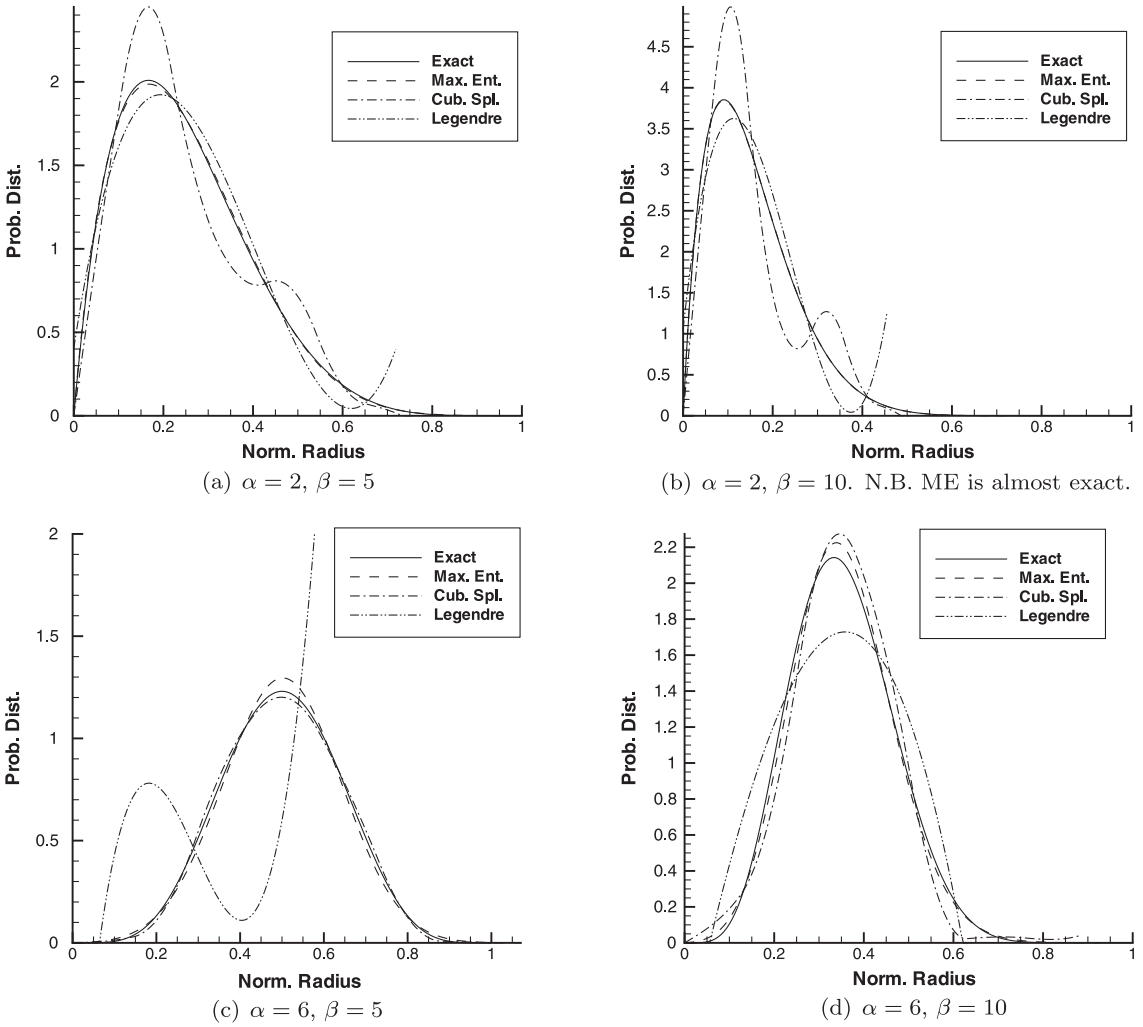

(a) $\alpha = 2,\ \beta = 5$ (b) $\alpha = 2,\ \beta = 10$. N.B. ME is almost exact.

(c) $\alpha = 6,\ \beta = 5$ (d) $\alpha = 6,\ \beta = 10$

Fig. 9. Distributions with positive skew using the first four moments.

Legendre method does produce a distribution, however at the supports, the magnitude of the gradients is large, producing a broad shape, unlike the other distributions.

From these first cases, the Maximum Entropy method performs consistently well, the cubic splines method produces poor reconstructions for the highly positively skewed cases and the Legendre method fails to produce a sensible distribution for the weakly skewed case.

Negative skew: The Maximum Entropy method and the cubic splines method in Fig. 10(a) both overpredict the peak and produce a tail on the right hand side, though still performing well. The Legendre method produces a near perfect approximation. Reducing the negative skew, Fig. 10(b) shows the Legendre method failing to produce a sensible approximation. This pattern continues as the variance is further reduced in Fig. 10(c) and (d). Only in Fig. 10(d) does the Maximum Entropy method show a slight advantage over the cubic splines method in approximating the height of the peak.

5.5.2. Bimodal

All methods manage to produce sensible reconstructions for bimodal distributions. Again, the Maximum Entropy method consistently performs the best, though the Legendre method produces almost identical distributions for all except that in Fig. 11(c). The cubic splines method produces wiggles in the distributions with large variances (Fig. 11(a) and (b)) and overshoots the peaks of the distributions with lower variances (Fig. 11(c) and (d)).

5.6. Unconditional solution

In the context of a CFD algorithm, the method for recovering the underlying distribution must be very reliable, that is, for a large range of possible moments which relate to a physically sensible distribution, the method will recover that

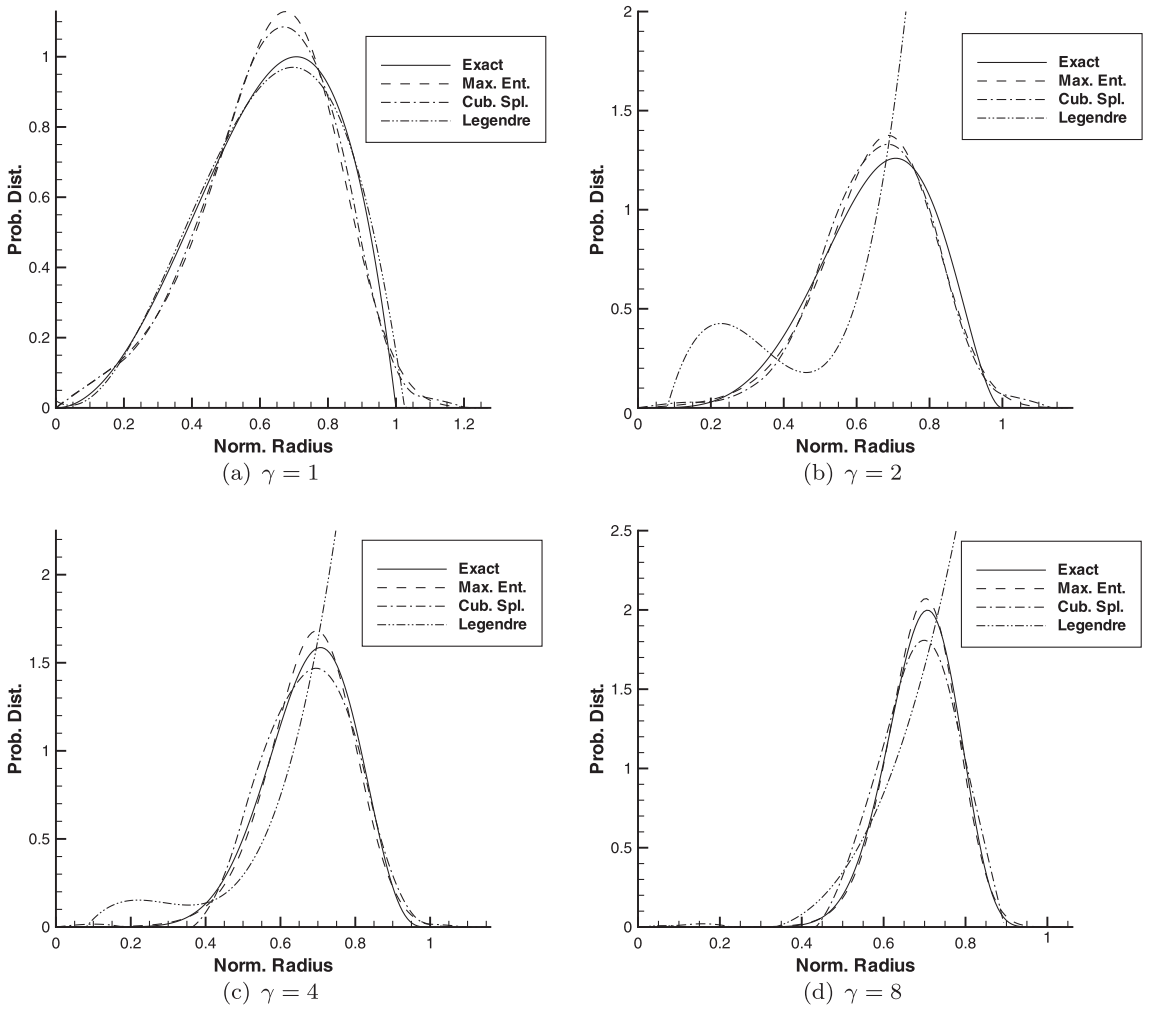

Fig. 10. Distributions with negative skew using the first four moments.

distribution. Of the cases given above, only one of these methods achieved that condition (at least for the range of cases considered) that is the Maximum Entropy method. This is not to conclude that other methods cannot produce reliable results for a range of cases (see [8] for examples of the Splines method), but given the computational time restriction preventing optimized free parameters being sought (especially in the Splines method), the Maximum Entropy method performs by far the best.

When running the different cases, the moments about the mean were calculated (from Eq. (4)). The purpose of this was to find a relationship between values of the moments about the mean and whether the closure method (in this case the Maximum Entropy method) converged or not. For this test only the first four moments were used. From 16 sample tests, for all cases, the following conditions were always met

$$\frac{\frac{r_{10}}{\sigma^2}}{\frac{\sigma^2}{|\gamma_1|}} = \frac{r_{10}|\gamma_1|}{\sigma^4} < 2.1 \tag{51}$$

and

$$\frac{r_{10}}{\sigma} > 1.1 \tag{52}$$

and the Maximum Entropy method always converged. These conditions make use of the mean, variance and skewness of the distribution, thus only require the first four moments. These then provide conditions which can be tested to determine whether the Maximum Entropy method should be called, or whether an alternative should be called if the condition is not met.

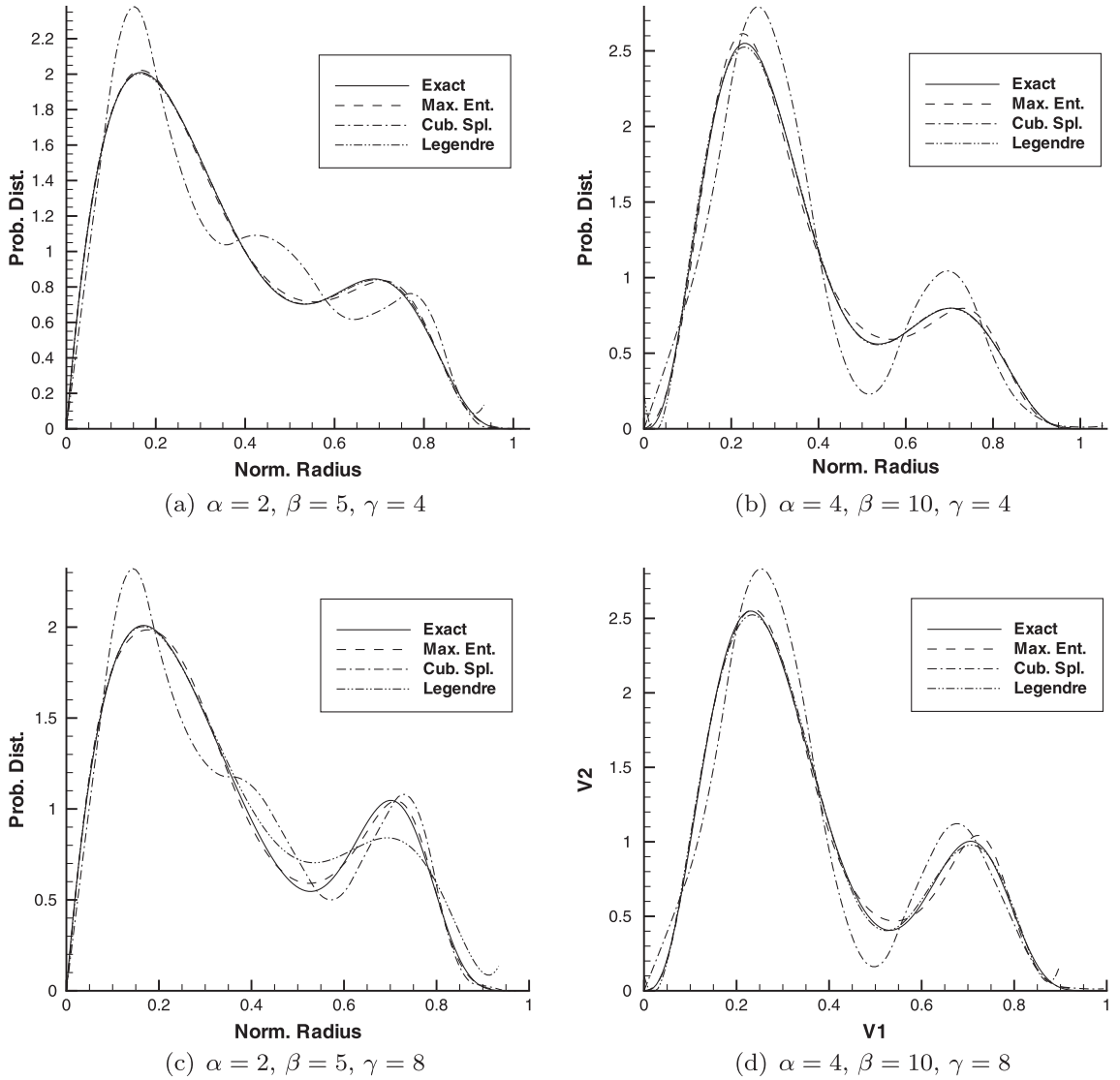

(a) $\alpha = 2,\ \beta = 5,\ \gamma = 4$ (b) $\alpha = 4,\ \beta = 10,\ \gamma = 4$

(c) $\alpha = 2,\ \beta = 5,\ \gamma = 8$ (d) $\alpha = 4,\ \beta = 10,\ \gamma = 8$

Fig. 11. Bimodal distributions using the first eight moments.

A priori methods can be forced to provide a solution by adjusting their parameters into the valid range if the parameters derived from the moments are out of range. This is a highly desirable quality, since such a method could be called if the conditions above are not met.

5.7. Optimal method

As suitable methods for determining the droplet distribution, two are feasible:

1. The Maximum Entropy method is set as the primary closure method, therefore moments from μ_0 must be transported. If closure by Maximum Entropy is not possible (Eqs. (51) and (52) are not met), the Gamma distribution is employed, using any choice of three consecutive moments, μ_i, μ_{i+1} and μ_{i+2}. The preferred choice would be when i is maximized.
2. The second choice is to use the Gamma distribution exclusively, thus only three moments are transported. This is the simplest method, and closure can be forced when necessary but can only generate a narrow range of unimodal distributions.

In the context of the spray model, transporting the first moment, μ_0, has been unachievable to date due to its relatively rapid decay compared to the transported higher order moments. With the inclusion in this model of a droplet velocity distribution, the problems associated with transporting μ_0 will hopefully be diminished.

Constructing the PDF using the Maximum Entropy method, as shown earlier, does not imply that the first moment, μ_0, must be known. However, attempts to solve the droplet number distribution failed. Only when the integral of the distribution was normalized to equal unity (using Eq. (47)) did the algorithm run successfully. In addition, if μ_0 is unknown, $p(r)$ must be set equal to one, preventing the solution from being accelerated and stabilized.

6. Assessment of droplet velocity profile methods

The first two proposed methods for constructing the velocity profile are presented here using point data obtained from running a sample spray simulation found in [9], whereby the simulation is run for a short duration, using the Maximum Entropy to construct the probability density function and the exponential function to construct the droplet velocity profile. Resulting droplet velocity profiles employing Maximum Entropy formalism are not presented here since no meaningful distributions were produced from the reference data. Implementation of this method requires further work.

Data from three points within the spray are taken: the first is close to the injector (point 1), the second is in the middle of the spray body (point 2) and the last is close to the inside edge of the spray (point 3). The extracted point data (the moments, continuum velocity and moment-averaged velocities) is shown in Table 3, with the corresponding PDFs at each point shown in Fig. 12.

6.1. Exponential function

The first method is presented in Fig. 13 at points 1–3 for a range of exponent values (0.2, 0.4 and 0.6). The index i in Eq. (41) is set as 3. At points 1 and 2, very similar shaped velocity profiles are found since the underlying PDFs are similar and the difference between the continuum and spray velocity at both points is also similar. For the third point, where the underlying PDF has strong positive skew, the droplet velocity picks up slower for the small droplets compared with the droplet velocities at points 1 and 2. For large exponents ($b \geqslant 0.4$) the velocity profile shows exaggerated values for the larger droplet size range compared with the corresponding moment-averaged velocities listed in Table 3.

Table 3
Extracted data from the spray.

Point	μ_0 (mm^{-3})	μ_1 (mm^{-2})	μ_2 (mm^{-1})	μ_3
1	18467.9	169.204	2.03169	0.0294586
2	6201.11	48.2283	0.482322	0.00561636
3	684.43	0.894604	0.00125258	2.70287E−05

	v (m/s)	$V_{d,0}$	$V_{d,1}$	$V_{d,2}$	$V_{d,3}$
1	37.4231	101.471	102.005	102.318	102.437
2	11.1468	74.447	68.5326	65.2815	67.5938
3	1.2158	66.7343	57.5367	50.7085	58.2257

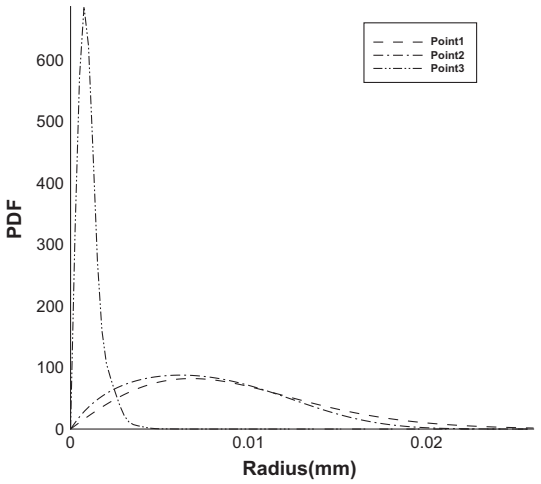

Fig. 12. PDFs from the extracted moments at points 1–3.

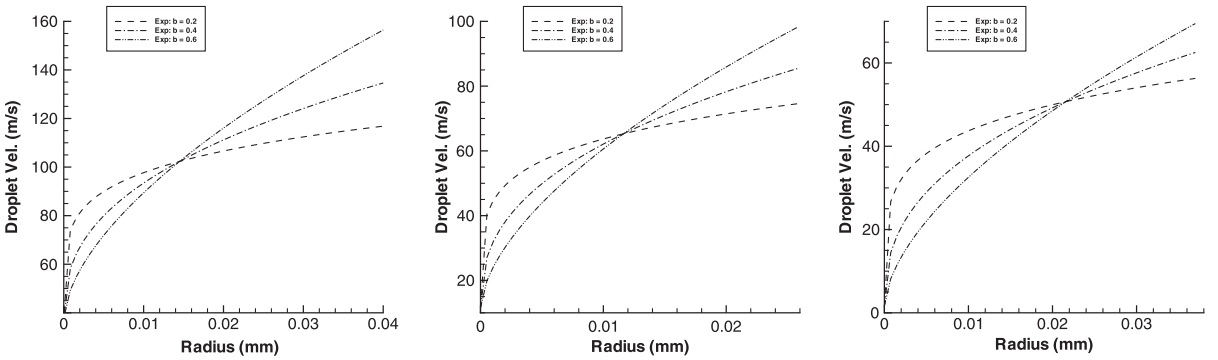

(a) Point 1 (b) Point 2 (c) Point 3

Fig. 13. Droplet velocity profile based on the exponential function.

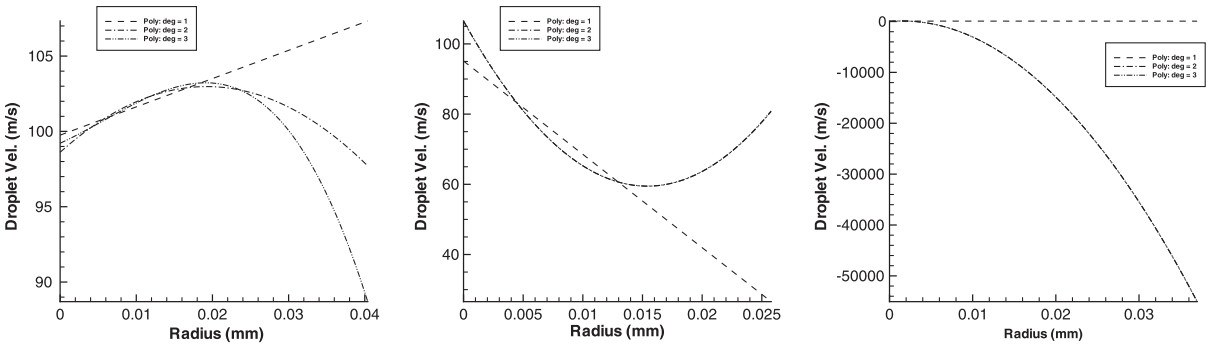

(a) Point 1 (b) Point 2 (c) Point 3

Fig. 14. Droplet velocity profile based on the polynomial function.

6.2. Polynomial function

The second method proposed has the capacity to make use of all the available moment averaged velocities to construct the droplet velocity profile, via a polynomial of a predefined degree. Fig. 14 shows that the profiles for the second and third degree polynomials are very similar (Fig. 14(a)) or near identical (Fig. 14(b) and (c)) indicating convergence of the profiles. However, only the parabolic velocity profile for point 2 (Fig. 14(b)) reflects the drop in the velocities for the intermediate moments, whereas the profiles for the remaining two points show no relation to the velocities they are based on.

The only possible use for this method is if only first degree polynomials are considered. However, the purpose of this method was to propose a means of using all the available moment velocities, which is shown to not be possible. For the spray model then, the first method will be adopted.

The unrealistic shape of the resulting profiles using polynomial functions is attributed to the kind of profile being solved. Unlike the PDF, the velocity profile does not have compact support. The problem this causes can be seen if the product of $\phi(r)$ and $v_d(r)$ were to be solved instead and then $v_d(r)$ recovered from the result. Unreliable values of $v_d(r)$ would be obtained when division of the resultant product by near-zero values of $\phi(r)$ is performed.

7. Conclusion

A review of droplet size distribution construction methods has been presented along with a wide range of comparative test cases, revealing the Maximum Entropy formalism to be the optimum choice for reconstruction, a conclusion which is quite different to that of [4]. Implementation details for the distribution methods have been discussed and an efficient algorithm for the numerical integration of batches of moments from the recovered distribution has been presented. To further advance this work, a cheap method for distributing the segmentation intervals optimally prior to obtaining the recovered distribution would permit the use of significantly fewer segmentations to retain the same resultant accuracy.

Approximating the droplet velocity profile is shown to be non-trivial. Of the methods presented only the exponential form offers sensible profiles so long as the exponent value b is limited to values less than 0.2. An alternative approach to

constructing a size distribution and a velocity profile is to construct a bivariate probability density function, $\psi(r, v_d)$. Methods for reconstructing such a distribution are found in [15,11,3,7,1], though the present spray model will need to be reformulated to make use of it. The development of this aspect of the work is the key to the success of a moments-based spray model. The simple exponential droplet velocity profile presented is somewhat contrived and its lack of a fixed upper-bound velocity readily exceeds its sensible range. Compact support must be the essential feature of any distribution used to further this work.

References

[1] R.V. Abramov, The multidimensional moment-constrained maximum entropy problem: a bfgs algorithm with constraint scaling, Journal of Computational Physics 228 (2009) 96–108.
[2] M. Ahmadi, R.W. Sellens, A simplified maximum-entropy-based drop size distribution, Atomization and Sprays 3 (1993) 291–310.
[3] D. Ayres, M. Caldas, V. Semiao, M. da Graca Carvalho, Prediction of the droplet size and velocity joint distribution for sprays, Fuel 80 (2001) 383–394.
[4] J.C. Beck, Computational modelling of polydisperse sprays without segregation into droplet size classes, Ph.D. Thesis, UMIST, 2000.
[5] J.C. Beck, A.P. Watkins, On the development of spray submodels based on droplet size moments, Journal of Computational Physics 182 (2002) 586–621.
[6] J.C. Beck, A.P. Watkins, On the development of a spray model based on drop-size moments, Proceedings of the Royal Society of London A (459) (2003) 1365–1394.
[7] M. Gurpura, Probability density function formalism for multiphase flows, Ph.D. Thesis, Iowa State University, 2007.
[8] V. John, I. Angelov, A.A. Oncul, D. Thevenin, Techniques for the reconstruction of a distribution from a finite number of its moments, Chemical Engineering Science 62 (2007) 2890–2904.
[9] D.P. Jones, Spray modelling without droplet size segregation, Ph.D. Thesis, University of Manchester, 2010.
[10] D.P. Jones, A.P. Watkins, Spray impingement model based on the method of moments, in: ILASS-Europe, 2008.
[11] R.W. Sellens, Prediction of the drop size and velocity distribution in a spray, based on the maximum entropy formalism, Particle Systems Characterization 6 (1989) 17–27.
[12] A. Tagliani, Numerical aspects of finite Hausdorff moment problem by maximum entropy approach, Applied Mathematics and Computation 118 (2001) 133–149.
[13] G. Talenti, Recovering a function from a finite number of moments, Inverse Problems 3 (1987) 501–517.
[14] B.K. Tay, G.B. McFiggans, D.P. Jones, M.W. Gallagher, C. Martin, A.P. Watkins, R.M. Harrison, Linking aerosol fluxes in street canyons to urban city-scale emissions, Atmospheric Chemistry and Physics 10 (2010) 2475–2490.
[15] A.D. Woodbury, A Fortran program to produce minimum relative entropy distributions, Computers and Geosciences 30 (2004) 131–138.
[16] B. Yue, A.P. Watkins, Mathematical development and numerical analysis of further transport equations for the droplet size moment theory, in: 19th Annual Meeting of the Institute for Liquid Atomization and Spraying Systems (Europe), 2004.